energies

MDPI

Article

The Coupling Fields Characteristics of Cable Joints and Application in the Evaluation of Crimping Process Defects

Fan Yang [1], Kai Liu [1,*], Peng Cheng [2], Shaohua Wang [3], Xiaoyu Wang [3], Bing Gao [1], Yalin Fang [1], Rong Xia [4] and Irfan Ullah [1]

1 State Key Laboratory of Power Transmission Equipment & System Security and New Technology, School of Electrical Engineering, Chongqing University, Chongqing 400044, China; dgjsxb80@sina.com (F.Y.); zhengke2015@sina.cn (B.G.); fly@cqu.edu.cn (Y.F.); irfan.ee@cqu.edu.cn (I.U.)

2 Chengdu Electrical Power Department, SiChuan Electrical Power Company, Chengdu 610041, China; zhaofuping2015@sina.cn

3 State Grid Zhejiang Electric Power Company, Hangzhou 310008, China; liurongmei2015@sina.cn (S.W.); zjdkylxp@sina.com (X.W.)

4 The Wuhan Branch of China Electric Power Research Institute, Wuhan 430071, China; jijing2014@sina.cn

* Correspondence: liukai2015@cqu.edu.cn; Tel.: +86-23-6511-1935

Academic Editor: Marco Marengo

Received: 14 September 2016; Accepted: 1 November 2016; Published: 9 November 2016

Abstract: The internal defects of cable joints always accelerate the deterioration of insulation, until finally accidents can arise due to the explosion of the joints. The formation process of this damage often involves changes in the electromagnetic, temperature and stress distribution of the cable joint, therefore, it is necessary to analyze the electromagnetic-thermal-mechanical distribution of cable joints. Aiming at solving this problem, the paper sets up a 3-D electromagnetic-thermal-mechanical coupling model of cable joints under crimping process defects. Based on the model, the electromagnetic losses distribution, temperature distribution and stress distribution of a cable joint and body are calculated. Then, the coupling fields characteristics in different contact coefficient k, ambient temperature T_{amb} and load current I were analyzed, and according to the thermal-mechanical characteristics of a cable joint under internal defects, the temperature difference ΔT_f and stress difference $\Delta\sigma_f$ of cable surface are applied to evaluate the internal cable joint defects. Finally, a simplified model of the cable joint is set up to verify the accuracy of the coupling field model proposed in this paper, which indicates that the model can be used to analyze the coupling fields characteristics of cable joints and the method can be applied to evaluate crimping process defects of cable joints.

Keywords: coupling fields; defects characteristics; temperature field; stress field; evaluation of internal defects; power cable joint

1. Introduction

With an ever greater number of power cables being used in urban power grids, more and more cable accidents occur every day [1–3], and cable joint explosions in particular are associated with great economic loses. The internal defects of cable joints are the main cause of explosions in cable joints. Explosions of cable joints happen due to internal defects that cause changes in the physical fields of cable joints, including electromagnetic fields [4,5], temperature fields [6,7] and stress fields [8–10]. Therefore, in order to protect the cable joints and avoid cable joint accidents, especially explosions, it is important to analyze the electromagnetic-thermal-mechanical characteristics of cable joints under internal defect conditions and find methods to evaluate the internal defects of cable joints [11].

The state of art work indicates that the electromagnetic fields of cables are an important factor to evaluate internal insulation nature of cable joints and they are widely used in the study of cable joints

for structure optimization and analysis of insulation [12,13]. Illias has investigated the electric field distribution of electric cable accessories under insulation defect conditions based on finite element analysis software [14,15]. Lachini has calculated the electric fields distribution of cables exposed to damp and analysed the influence of relevant parameters on cable joints [16]. However, the statistical data of the cables industry in China has showed that an insufficient amount of surface stress on cable joints are also one of the major causes of explosions of cable joints [17,18]. Hence, to understand the surface stress distribution of cable joints is a significant factor for the evaluation of the internal defect states of cable joints. Yoshida [19] applied a pressure sensor to measure the stress distribution of cables and analysed the influence of relevant parameters. However, there are fewer studies on the characteristic distribution of electromagnetic fields or stress fields on cable joints under crimping process defects and there is still no efficient method for evaluating the crimping process defects of cable joints.

On the other hand, power cables will produce heat losses during operation, which causes an increase of the cable internal temperature and overheating, when internal defects exist in the cables. Hence, the cable temperature is also an important parameter to evaluate the internal states of cables. The current research shows that there are many techniques for the thermal analysis of power cables, which can be divided into two main methods: the numerical methods [6,20] and the methods based on IEC-60287 [21]. Olsen proposed a unique calculation method for the dynamic temperature of cables which can consider the changes of ambient thermal resistance and specific heat in the time domain [7]. Sedaghat calculated the steady-state temperature distribution of cables in free air and improved the method for the calculation of the current carrying capacity based on the IEC standards [22]. Canova investigated the transient and steady-state thermal behavior of cables [23]. Anders build an analytical model for the calculation of cables' current carrying capacity in air-filled troughs [24]. James has proposed a new technique to calculate the cable ratings based on computational fluid dynamics [25]. The above discussed techniques are mainly focused on the computation of cable ratings and neglect the heat transfer in cable joints. In reference [26], the authors proposed using the temperature of cable joints to evaluate their contact resistance, but did not find comprehensive results in research community. For example, when cables are working for a long time, the temperature of the cables are higher than the normal temperature, and the temperature cannot be applied to evaluate the state of cables at same time, so we hope to find some comprehensive and efficient methods to evaluate the internal defects of cable joints.

Aiming at solving the above problem, based on the fundamentals of the electromagnetism, heat transfer theory and mechanics, this paper sets up a 3-D coupling field computation model of cable joints, and the electromagnetic fields, temperature fields and stress fields of a cable joint under internal defects are calculated based on this model. Then, the influences of internal defects on the temperature field and stress field of cable joints are considered through the equivalent conductivity of cable joints, and the coupling fields characteristics for different values of the contact coefficient k, ambient temperature T_{amb} and load current I are discussed. Moreover, based on the thermal-stress characteristics of cable joints, this paper proposes an evaluation method for the internal defects of cable joints combining their temperature and stress distributions. Finally, a simplified model of cable joints is set up to verify the accuracy of the proposed coupling fields model.

2. The Coupling Field Analysis Model of Cable Joints under Crimping Process Defects

2.1. The Physics Fields Computation of Cable Joints

A cold-shrinkable joint of a 8.7/15kV YJV 1 × 400 XLPE power cable was discussed in [26], and its structural parameters are the following: the conductor diameter is 23.8 mm, the thickness of the insulating layer is 4.5 mm, the thickness of the metallic shield is 0.5 mm, the thickness of the outer sheath is 2.5 mm, the thickness of the cable outer diameter is 41 mm, and its axial section in shown in Figure 1a. The closed region model of physics fields calculation for the cable joints is shown in

Figure 1b. Here, calculations are still based on the model to analyze the coupling fields of cable joints under crimping process defect conditions.

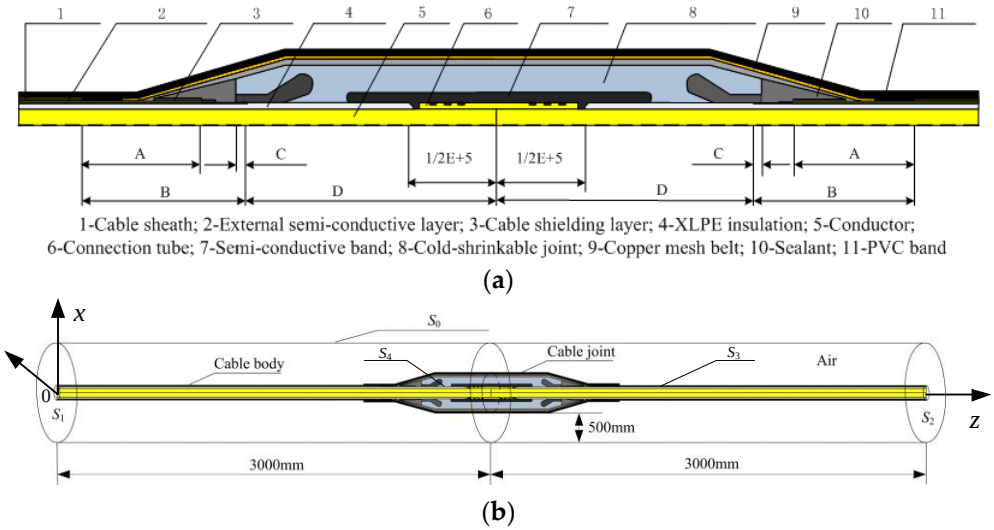

Figure 1. The model of a cable joint, (**a**) The axial section model of cable joint; (**b**) The closed region calculation model for cable joint.

According to [26], the electromagnetic fields and the steady-state heat conduction equations of cable joints can be described as follows:

$$\begin{cases} (\nabla \cdot \frac{1}{\mu}\nabla)A = -J_s + j\omega\sigma A \\ A\big|_{S_0} = 0 \\ n \times A\big|_{S_1S_2} = 0 \end{cases} \tag{1}$$

$$\begin{cases} \nabla \cdot (\lambda \nabla T) + Q_v = 0 \\ -\lambda \frac{\partial T}{\partial n}\Big|_{S_3} = (h + h_r)(T_f - T_a) \\ \lambda \frac{\partial T}{\partial n}\Big|_{S_1S_2} = 0 \end{cases} \tag{2}$$

where μ is the permeability, A is the magnetic vector potential, σ is the conductivity of cable joint, J_s represents the applied current density, ω is the angular frequency, n represents the boundary normal vectors, λ is the thermal conductivity, T is the temperature, Q_v is the heat source per unit volume, h is the coefficient of convective heat transfer, h_r is the coefficient of radiation heat transfer, $h_r = \frac{\sigma_0 \varepsilon (T_f^4 - T_{amb}^4)}{T_f - T_a}$, T_a is the temperature of air, T_f represents the surface temperature, T_{amb} is the environment temperature, $\sigma_0 = 5.67 \times 10^{-8}$ is the Stefan-Boltzmann constant, ε is the surface emissivity. The main equation of thermal-mechanical for the cable joints is described in Equation (3):

$$\begin{cases} \frac{\partial \theta_{ij}}{\partial x_j} + f_i = \rho \frac{\partial^2 u_i}{\partial t^2} + \gamma \frac{\partial u_i}{\partial t} \\ \eta_{ij} = \frac{1}{2}(\frac{\partial u_i}{\partial x_j} + \frac{\partial u_j}{\partial x_i}) \\ \eta_{ij} = \eta_{ij}^E + \eta_{ij}^{Th} \\ \theta_{ij} = D_{ijkl}\eta_{kl}^E \\ \eta_{ij}^{Th} = \alpha \Delta T \delta_{ij} \end{cases} \tag{3}$$

where θ is the stress tensor, f is the externally applied force, ρ is the material density, u is the displacement, t is the time, γ is the damping coefficient, η is the strain tensor, η^E is the elastic strain component, η^{Th} is the thermal strain component, D is the strain coefficient, α is the linear expansion

coefficient, ΔT is the temperature difference compared with reference temperature, $i = j = k = l = 1, 2, 3$, and the fourth-order tenstor D can be expressed by the following equation:

$$D_{ijkl} = \frac{E(T)}{1+v}\delta_{ik}\delta_{jl} + \frac{E(T)}{(1+v)(1-2v)}\delta_{ij}\delta_{kl} \tag{4}$$

where $E(T)$ is the Young's modulus of material, v is the Poisson's ratio of material, δ_{ij} is described by:

$$\delta_{ij} = \begin{cases} 1, & i = j \\ 0, & i \neq j \end{cases} \tag{5}$$

Studies have shown that there must be a grasping force between the cable accessories and the major insulation bonding interface in order to avoid the surface flashover of cable accessories without installation difficulty and insulation failure of the cables, so the grasping force boundary conditions on the bonding interface can be expressed by the equation below:

$$n \cdot \sigma \big|_{S_4} = f_0 \tag{6}$$

Generally, the initial surface stress on bonding interface must reach 0.25 MPa for new cable joints, and f_0 = 0.25 MPa. By only considering the radius of heat transmission, the displacement of the cable on section S_1, S_2 is also along radial direction, and the axial components are 0, the boundary conditions are as follows:

$$n \cdot u \big|_{S_1, S_2} = 0 \tag{7}$$

The boundary conditions on surface of cable joints are boundary free, and there is no constraint conditions for external forces and displacements.

2.2. The Equivalent Model of Cable Joint under Crimping Process Defects

Due to the problems of manufacturing condition and human errors, crimping process defects appear in cable joints and there will exist a contact resistance between the cable body and the connection tube, which will cause an increase of the cable joints' internal temperature when current flows through the joints. Therefore, the contact resistance must be considered when analyzing the temperature at the junctions, which is the reason that the thermal loss of cable joints under crimping process defects must be considered.

According to Equation (1), when analyzing the electromagnetic fields of cable joints, the input parameters are the electrical conductivity and magnetic conductivity of materials. Hence, in order to consider the effect of contact resistance for temperature rises, the electromagnetic heat loss of cable joints can be calculated by calculating the equivalent conductivity between the cable body and connection tube. The structure and equivalent simulation model of cable conductor junctions are shown in Figure 2, S_1–S_5 are respectively the five contact surfaces where contact resistance exists, r_1 and σ_1 are respectively the conductivity radius of the cable, σ_2 is the equivalent conductivity at the junction, r_2 and l are the outer radius and length, respectively. We can assume that R_1 is the resistance of connection and R_2 is the conductor resistance of cable body with the same length.

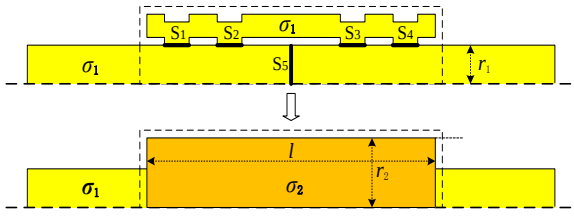

Figure 2. Structure and equivalent model of a cable joint junction.

$$R_1 = l/\left(\sigma_2 \cdot \pi \cdot r_2^2\right) \tag{8}$$

$$R_2 = l/\left(\sigma_1 \cdot \pi \cdot r_1^2\right) \tag{9}$$

If the contact coefficient is written as k, it can be described as:

$$k = \frac{R_1}{R_2} = \frac{\frac{1}{\sigma_2} \cdot \frac{l}{\pi \cdot r_2^2}}{\frac{1}{\sigma_1} \cdot \frac{l}{\pi \cdot r_1^2}} = \frac{\sigma_1}{\sigma_2} \cdot \left(\frac{r_1}{r_2}\right)^2 \tag{10}$$

so that:

$$\sigma_2 = \frac{\sigma_1}{k} \cdot \left(\frac{r_1}{r_2}\right)^2 \tag{11}$$

Therefore the value of the contact coefficient k can reflect the contact resistance and the internal defects of cable joints. According to Equation (8), if the contact resistance between the cable body and connection tube is neglected and $\sigma_1 = \sigma_2$, it is known that $k < 1$, which is an ideal case. However, in practical engineering, the k will be always greater than 1 due to the existence of contact resistance, and when defects exist in the crimping process of cables, the k value will be greater than 1. Therefore, this research work considers those cases when $k = 1$ or $k > 1$.

According to the above definition, it is clear to conclude that:

$$\begin{cases} R_J \approx 0 \quad \sigma_1 \approx \sigma_2 \quad R_1 < R_2 \quad and \quad k < 1 & \text{for qualified cable joints} \\ R_J > 0 \quad \sigma_1 < \sigma_2 \quad R_1 > R_2 \quad and \quad k \geq 1 & \text{for unqualified cable joints} \end{cases} \tag{12}$$

2.3. The Coupling Field Computation of Cable Joints under Crimping Process Defects

In this research the multi-physical fields coupling of cable joints includes in particular the electromagnetic-thermal coupling and thermal-mechanical coupling, and the coupling relationship between electromagnetic field, thermal field and stress field is shown in Figure 3.

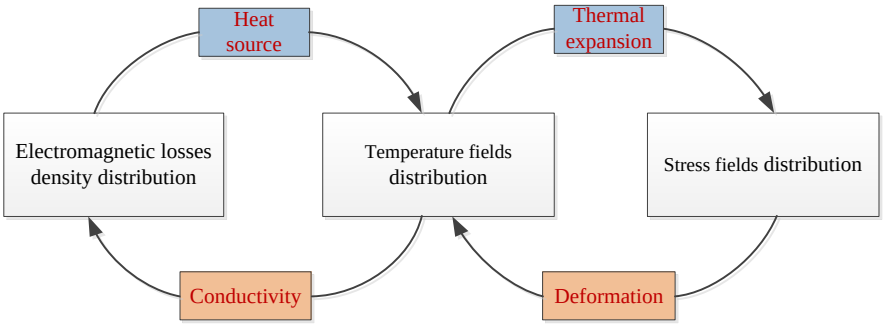

Figure 3. Coupling relationship of the electromagnetic-thermal-mechanical fields.

The coupling between electromagnetic fields and thermal fields is related to two-way coupling. When calculating the temperature distribution by Equation (2), the heat source term Q_v depends on the electromagnetic losses density of cable joints. On the other hand, the electromagnetic loss density of cable joints depends on the conductivity of cable joints, and the conductivity of cable joints has a correlation with the temperature of cable joints. This can be described as follows:

$$J = \nabla \times \frac{1}{\mu} \nabla \times A \tag{13}$$

$$Q_v = \frac{1}{\sigma}|J|^2 \tag{14}$$

$$\sigma = \frac{\sigma_{20}}{1 + \alpha(T - 20)} \tag{15}$$

where J is the total current intensity, σ_{20} is the conductivity at 20 °C, S/m; α is the temperature coefficient, 1/°C; T is the cable conductor temperature, °C.

The coupling between thermal fields and stress fields also belongs to two-way coupling. When calculating the stress field by Equation (3), the displacement distribution and temperature distribution of each computing element must be known. However, the deformation caused by the changes of stress field of cable joints will influence the temperature distribution. The one-way coupling process from temperature field to stress field can be described as below:

$$\varepsilon^{Th} = \alpha \Delta T = \alpha(T - T_{ref}) \tag{16}$$

where ε^{Th} is the thermal strain component, D is the strain coefficient, α is the linear expansion coefficient, ΔT is the temperature variation compared with reference temperature, T is temperature of cable joints, T_{ref} is reference temperature.

Combining the coupling of electromagnetic fields, temperature field and stress field of cable joints, this research work uses secondary development of finite element software COMSOL and hybrid programming to calculate the electromagnetic-thermal-mechanical coupling fields, and the calculation flow chart is shown in Figure 4.

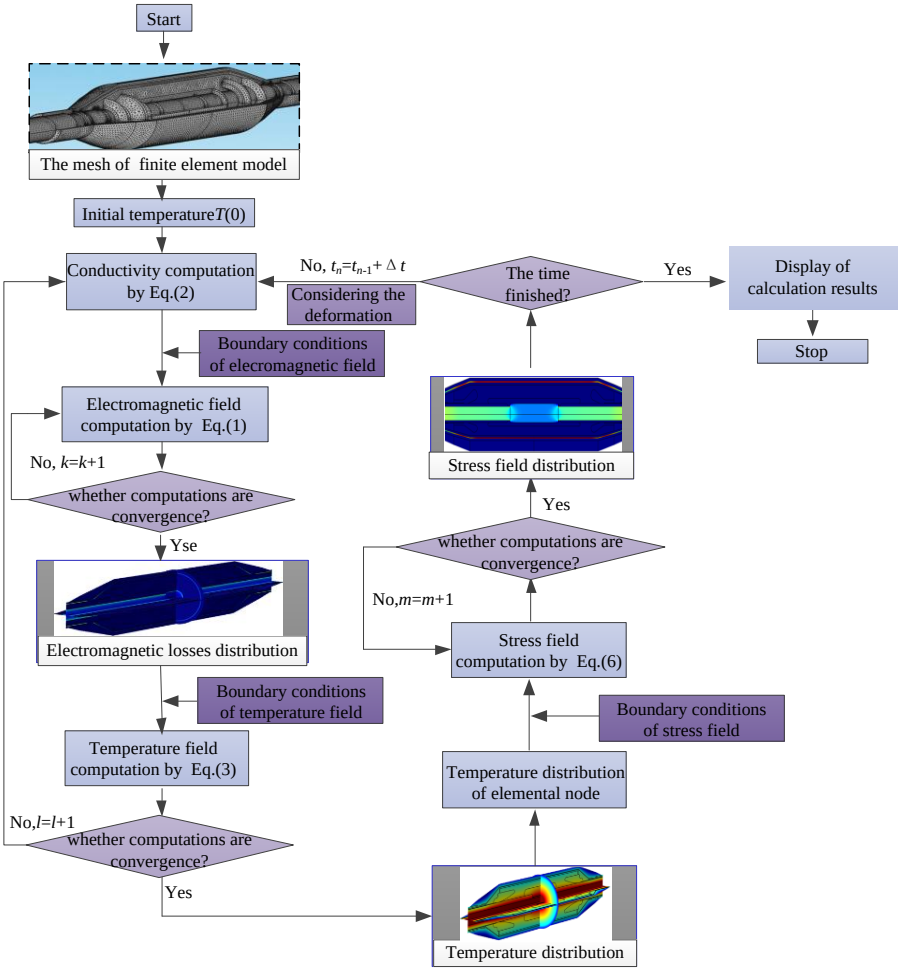

Figure 4. Calculation flow chart of electromagnetic-thermal coupling model.

2.4. Example Calculation

Based on the 3-D coupling field analysis model, the electromagnetic losses distribution, temperature distribution and stress distribution of the 8.7/15 kV YJV 1 × 400 XLPE cable can be calculated. The structure parameters of the cable are as follows: the ambient temperature is 25 °C, the convective heat-transfer coefficient is 5.6 W/(m^2·K), and the surface emissivity is 0.6. For good computing precision, the cable joints are subdivided by tetrahedral meshes and uneven mesh as shown in Figure 5.

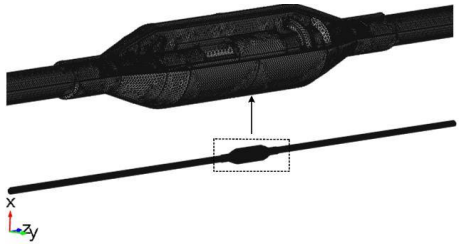

Figure 5. 3-D finite element mesh of cable joint model.

When the load current I is 645 A and k is 5.0, the 3-D electromagnetic losses distribution of the cable joint are shown in Figure 6.

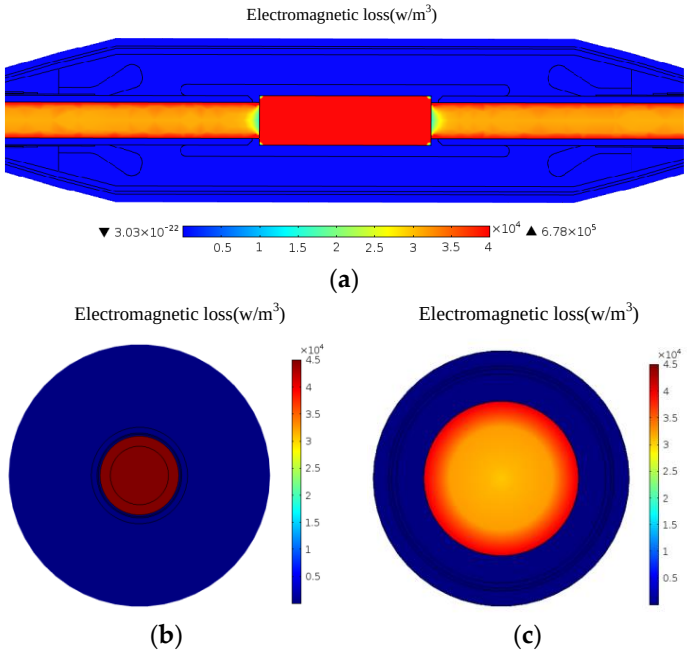

Figure 6. 3-D electromagnetic losses distribution of cable, (**a**) 3-D electromagnetic losses distribution of joint; (**b**) Electromagnetic losses distributions on cable joint axial section; (**c**) Electromagnetic losses distributions on cable body axial section.

It can be seen from Figure 6 that the electromagnetic losses distribution in the conductor is irregular, as the electromagnetic losses of the outer surface is greater than on the inner side. That effect is because of the skin effect which causes the current density to mainly focus on the conductor surface, which can be also seen from Equation (11). Since the equivalent conductivity of the cable body surface is higher than that of the cable joint, the skin effect for the cable joint is less sensitive, which causes the electromagnetic losses of the cable joint to increase. Figure 6 shows that the electromagnetic losses of the cable joint cross-section is 82.8 W/m which is 4.85 times greater than from the body of the cable.

The electromagnetic losses distribution of the cable joint can be coupled into the temperature field analyzing module to calculate the temperature distribution of the cable joint, as shown in Figure 7.

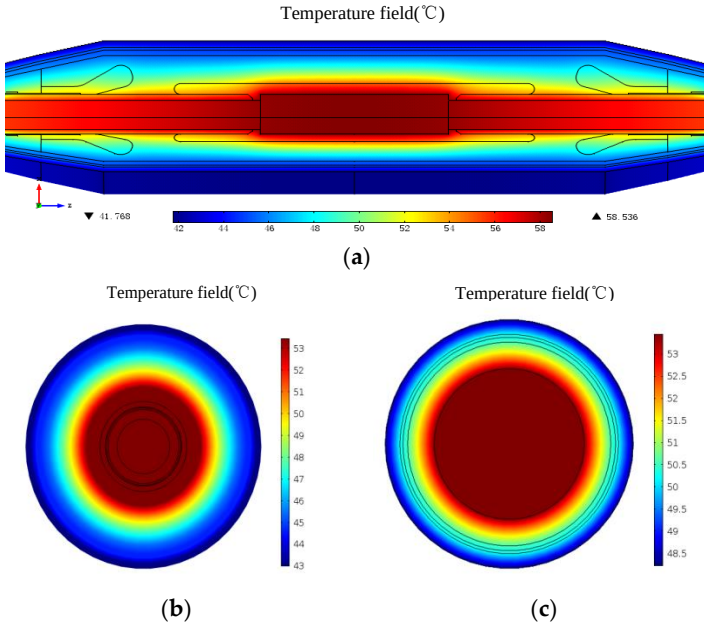

Figure 7. 3-D temperature field distribution of cable, (**a**) 3-D temperature distributions of cable joint; (**b**) Temperature distributions on cable joint axial section; (**c**) Temperature distributions on cable body axial section.

Figure 7 shows that the cable joint has a larger surface area than the cable body, which makes the cable joint have the stronger heat dissipation capacity, hence the maximum surface temperature of the cable body is 6.4 °C higher than that of the cable joint, which shows that the temperature conditions remain constant with the electromagnetic loss distribution for the cable joint.

The simulation results of temperature distribution can be coupled into the stress field calculation module to calculate the steady-state stress field distribution of the cable joint, as shown in Figure 8.

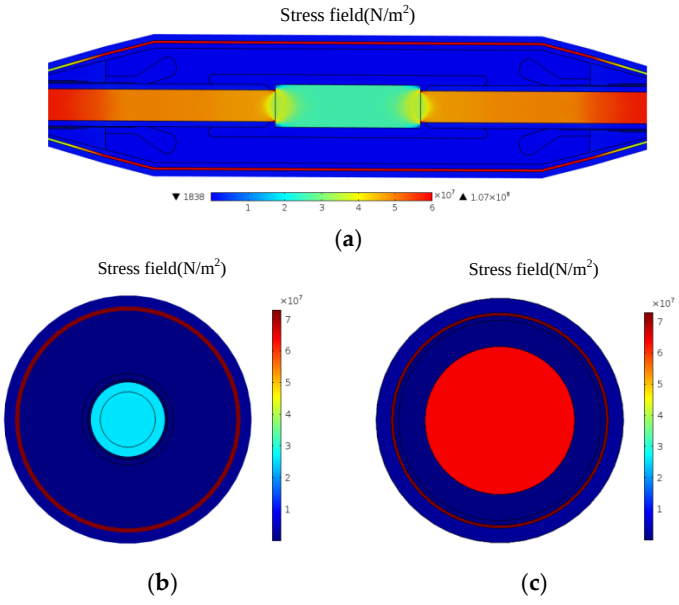

Figure 8. Axial stress distribution of cable, (**a**) 3-D stress field distribution of cable joint; (**b**) Stress distributions on cable joint axial section; (**c**) Stress distributions on cable body axial section.

Figure 8 shows that the maximum stresses of the cable joint and cable body are 9.5665×10^7 N/m^2 and 7.2887×10^7 N/m^2, respectively, which both appear on the metallic shield. This phenomenon occurs because the inner insulation layers and outer sheath will reproduce the stress on the metallic shield after it expands by heat. It can be also seen from Figure 8 that the stress of the cable joint is less than the stress of the cable body due to the inner stress generated by the highly elastic prefabricated rubber material on the outside of cable joint conductor after it expands with the heat and the stress on the outside of the cable body is less than in the cable joint.

3. Analysis of Thermal-Mechanical Characteristics under Crimping Process Defects

In the above discussion, the contact resistance of a cable joint under crimping process defects is considered through solving the equivalent conductivity of the cable joint and introducing the contact coefficient "*k*". Then, the electromagnetic-thermal-mechanical distribution under crimping process defects is calculated. Here the influence effects of thermal-mechanical characteristics will be discussed.

3.1. Analysis of Thermal Characteristics

3.1.1. The Influence of Contact Coefficient *k*

Keeping I = 645 A and T_{amb} = 25 °C constant, the axial surface temperature field distribution of cable with different contact coefficients can be calculated, as shown in Figure 9.

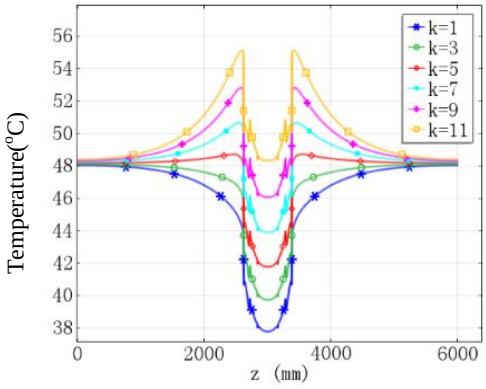

Figure 9. Axial surface temperature field distribution of cable with different contact coefficients.

The following can be concluded from Figure 9:

The axial surface temperature of the discussed cable joint rises with the increase of contact coefficient k and the increase rate will be slight. When k changes from 1 to 3, the highest surface temperature rises from 37.77 °C to 39.89 °C for an increase of 2.12 °C. On the other hand, when k changes from 9 to 11, the highest surface temperature rises from 46.19 °C to 48.48 °C and has an increase of 2.29 °C.

When z < 500 mm and z > 5500 mm, the thermal conduction along the axis is weak, which causes the axial temperature of cable surface to remain constant with increase of k at z < 500 mm and z > 5500 mm.

When k < 11, the surface heat dissipation of the cable joint is dominant, so the surface temperature of the cable body is higher than that of the cable joint. When k = 11, the balance between surface heat absorption and surface heat dissipation of cable joint reaches the level of the cable body, which causes the surface temperature of the cable joint to be the same as that of the body of the cable.

3.1.2. The Influence of Ambient Temperature T_{amb}

Keeping I = 645 A and k = 5 constant, the axial temperature field distribution of the cable surface with different ambient temperatures can be calculated, as shown in Figure 10. From Figure 10 the following conclusions can be obtained:

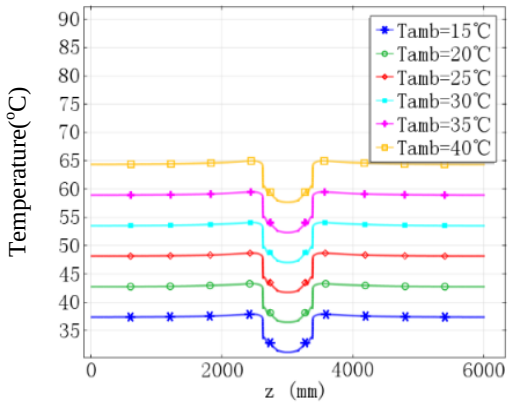

Figure 10. Axial temperature field distribution curves of cable surface with different ambient temperatures.

The axial temperature of the cable surface will rise with the increase of ambient temperature T_{amb}. The increase rate remains constant with the increase of T_{amb}, and the axial temperature of cable surface will increase 1.12 °C when the ambient temperatures T_{amb} increases by 1 °C.

The difference of axial temperature of the cable surface at z = 5500 mm and z = 3000 mm is less affected by the ambient temperatures T_{amb}, and the difference is about 6.45 °C.

3.1.3. The Influence of Load Current *I*

Keeping k = 5 and T_{amb} = 25 °C constant, the axial temperature field distribution of the cable surface with different load currents can be calculated as shown in Figure 11.

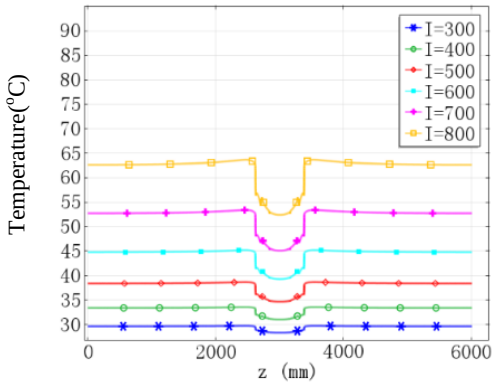

Figure 11. Axial surface temperature field distribution of cable with different load currents.

Figure 11 shows that the axial temperature of the cable surface will increase with the increase of load currents I, and the increase rate shows a rise with increase of I. For cable conductor, when the current I changes from 300 A to 400 A, the temperature of the cable conductor at z = 3000 mm and z = 5500 mm have increases of 5.41 °C and 4.61 °C, respectively. When current I changes from 700 A to 800 A, the temperature of the cable conductor at z = 3000 mm and z = 5500 mm has increases of 14.54 °C and 12.08 °C, respectively.

3.2. Analysis of Stress Characteristics

3.2.1. The Influence of Contact Coefficient *k*

The contact coefficient k of a cable joint will directly affect the temperature distribution of the cable joint, and it is also the most important factor affecting the stress distribution of the cable joints.

If the contact coefficient k is higher and the temperature of cable joints is also higher at the same time, then the stress of cable joints is higher, and vice versa. When I = 645 A and T_{amb} = 25 °C, the axial stress field distribution of cable surface with different contact coefficient can be calculated as shown in Figure 12.

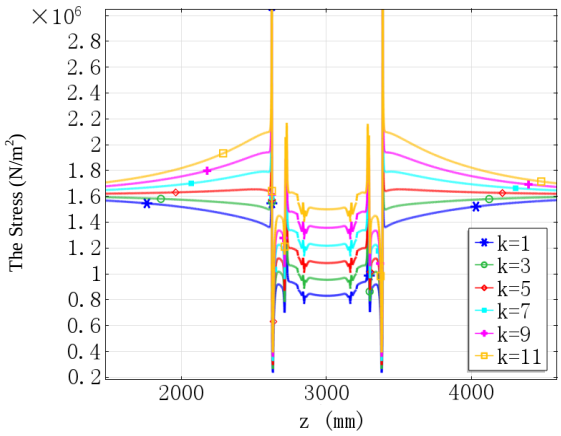

Figure 12. Axial stress field distribution curves of cable surface with different values of contact coefficients.

It can be seen from Figure 12 that the axial stress of cable surface and cable conductor rises with the increase of contact coefficient k and the increase rate will rise to some extent. The cable surface is open boundary, and the surface stress field distribution of the cable is mainly affected by the temperature. Therefore, the stress distribution of cable surface is constant with the temperature distribution. It can be seen from Figure 12 that the contact coefficient k has little effect on the surface stress of cable body at z = 5500 mm, in other words, the internal defects in the cable joint have little effect on the surface stress of the cable body.

3.2.2. The Influence of Ambient Temperature T_{amb}

When the ambient temperature T_{amb} and the temperature of the cable are higher, the stress of the cable joint is also higher, and vice versa. When I = 645 A and k = 5, the axial stress field distribution of the cable surface with different ambient temperatures can be calculated as shown in Figure 13.

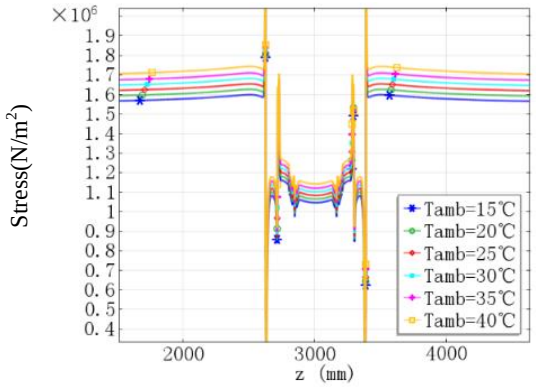

Figure 13. Axial surface stress field distribution of cable with different ambient temperatures.

Figure 13 shows that the axial stress of the cable surface will increase with the increase of ambient temperature T_{amb}. The increase rate remains constant with increase of T_{amb}. The difference of axial

stress of the cable surface at z = 5500 mm and z = 3000 mm is less affected by the ambient temperatures T_{amb}, and the difference is almost constant.

3.2.3. The Influence of Load Current I

The load current I has a direct effect on the temperature of the cable, so it is also an important additional factor affecting the stress distribution of cable. When the load current I increases, the temperature of the cable body and cable joint will rise, respectively, which causes an increase in the stress of the cable body and cable joint. Considering that T_{amb} = 25 °C and k = 5 remain constant, the axial stress field distribution of the cable surface with different load currents can be calculated as shown in Figure 14.

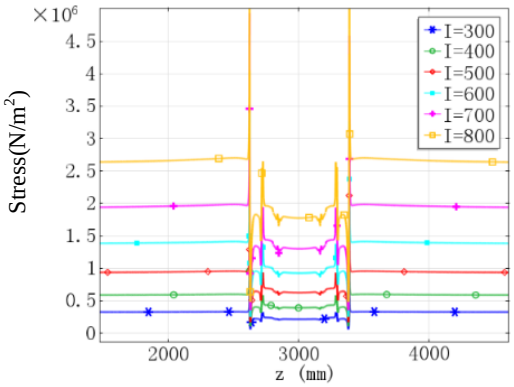

Figure 14. Axial stress field distribution curves of cable surface with different load currents.

Figure 14 shows that the axial stress of cable surface will rise with the increase of load currents I, and the increase rate rises as I increases. When the current I changes from 300 A to 400 A, the stress of the cable surface at z = 3000 mm and z = 5500 mm has increases of 4.108 × 10^6 N/m^2 and 1.0457 × 10^7 N/m^2, respectively. When the current I changes from 700 A to 800 A, the stress of the cable conductor at z = 3000 mm and z = 5500 mm have increases of 1.0876 × 10^7 N/m^2 and 2.774 × 10^7 N/m^2, respectively.

4. Evaluation of Internal Defect States of Cable Joint under Crimping Process Defects

The forward problem and inverse problem of cable joints under internal defects is shown in Figure 15. If we consider the above analysis of thermal-stress characteristics as the forward problem, this evaluation of defect states of cable joints can be considered as the inverse problem analysis, and the internal defect states of cable joints can be obtained by measuring characteristic parameters such as temperature and stress of cable joint under internal defects, which provides a new method to diagnose the internal defects of cable joints.

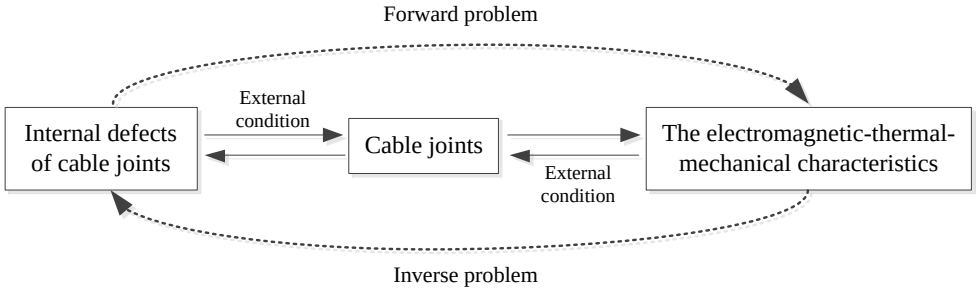

Figure 15. Forward and inverse problem analysis of the cable joint under internal defects.

If there exist crimping process defects in cable joints, the contact resistance between the cable body and the connection tube will increase, and in the discussion above the contact coefficient k has been introduced to characterize the contact resistance of cable joints under crimping process defects. Therefore, the evaluation of internal defect states of cable joints can be turned into the evaluation of the contact coefficient k.

4.1. Evaluation Results and Analysis Based on Temperature Characteristic

It can be proved from the above analysis that the temperature of cable joints will be affected by the contact resistance k, ambient temperature T_{amb} and load current I, but the surface temperature difference of the cable at z = 3000 mm and z = 5500 mm only depends on k, and I, and is not affected by the ambient temperature T_{amb}. Therefore, in order to reduce the complexity of the characterization method, we can select the temperature difference ΔT_f of the cable surface and load current I as the feature variables to evaluate the value of k and identify the internal defects of cable joints.

Based on the above computation model proposed by this paper, more calculations are carried out to obtain large amounts of data (I, k, ΔT_f) with k from 1 to 10 and I from 300 A to 1000 A, and these data are drawn as the 2-D colored contour shown in Figure 16.

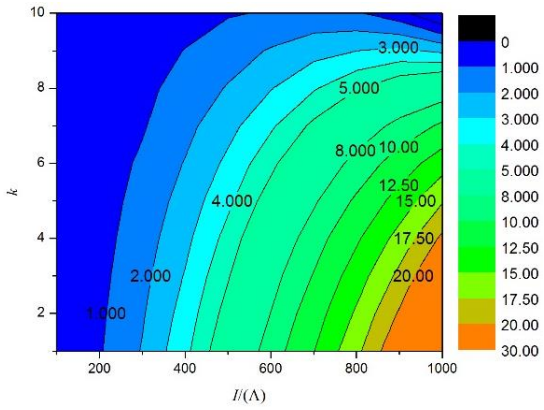

Figure 16. 2-D colored contour of temperature data with different values of ratio k and load current I.

The mathematical formulation of the fitting process is done on the data in Figure 16 by selecting different functions, and the optimal expression of the fitting function can be obtained as shown in Table 1, and the correlation coefficient is as high as 0.99115. According to this expression, the 2-D colored contour of k, I and ΔT_f can be draw as shown in Figure 17, and the results are almost similar to the result shown in Figure 16.

In engineering practice, for the cables without an internal optical fiber temperature sensor, if the T_f and I of the cable can be measured, the contact resistance of the cable joints can be evaluated by the expression shown in Table 1 or by using a graphical method, as described below.

In first stage, the surface temperatures of the cable body T_{bf} and the surface temperatures of the cable joint T_{jf} should be measured, and the temperature difference ΔT_f between T_{bf} and T_{jf} can be calculated $\Delta T_f = T_{bf} - T_{jf}$, here assuming ΔT_f = 3 °C.

In the second stage, the real-time load current of the cable can be obtained according to the data for cable operation, here assuming the current is I = 500 A.

In the final stage, putting the surface temperature difference ΔT_f = 3 °C and I = 500 A into the fitting function shown in Table 1, the contact coefficient k can be calculated and k = 5.7.

We can also use graphical method to evaluate the contact coefficient k. For example, as shown in Figure 17, we can draw a vertical line at I = 500 A to intersect the ΔT_f = 3 °C isotherm at A, then draw a horizontal line to pass through point A and intersect the ordinate at B, and read the value of k at point B and k = 5.7.

Table 1. Expression of the fitting function of ΔT_f, k and I.

Equation	$\Delta T_f = A + 0.25B\left[1+\text{erf}\left(\frac{I-C}{\sqrt{2}D}\right)\right]\left[1+\text{erf}\left(\frac{k-E}{\sqrt{2}F}\right)\right]$
Parameters	A = 0.06123 B = 66.23295 C = 1051.6936 D = 414.48237 E = 5.62593 F = −3.13981
Correlation coefficient	0.99115

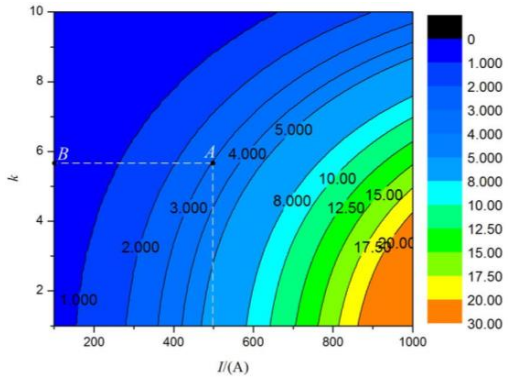

Figure 17. 2-D colored contour of ΔT_f with different k and I values obtained by fitting.

4.2. Evaluation Results and Analysis Based on Stress Characteristic

The temperature of cable joints as a unique characteristic which is very difficult to evaluate and effectively detect the internal defects of cable joints. Therefore, this paper has proposed an evaluation method through combining the temperature and stress field distribution of cable joints. The stress difference is also applied to evaluate the contact resistance and internal defects of cable joints based on the stress characteristics under crimping process defect conditions. The detailed process based on stress characteristics is similar to the temperature one which is explained in Section 4.1, which needs not be repeated. Here, the optimal equation of the fitting function can be shown in Table 2 and the correlation coefficient is as high as 0.9965. According to this equation in Table 2, the 2-D colored contour of k, I and ΔT_f can be draw, as shown in Figure 18.

Table 2. Equation of the fitting function of $\Delta\sigma_f$, k and I.

Equation	$\Delta\sigma_f = A + 0.25B\left[1+\text{erf}\left(\frac{I-C}{\sqrt{2}D}\right)\right]\left[1+\text{erf}\left(\frac{k-E}{\sqrt{2}F}\right)\right]$
Parameters	A = 0.0052 B = 5.16572 C = 1041.9008 D = 411.43753 E = 6.06807 F = −4.33966
Correlation Coefficient	0.9965

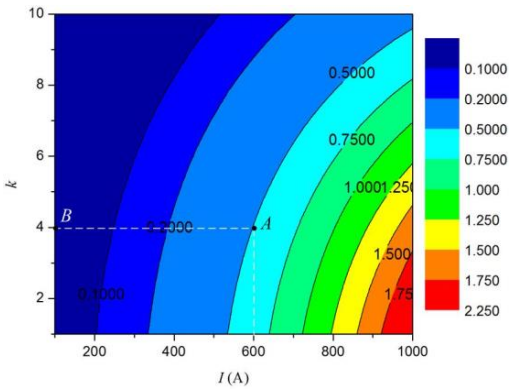

Figure 18. 2-D colored contour of $\Delta\sigma_f$ with different k and I values obtained by fitting.

In engineering operation, the contact resistance of the cable joints can be evaluated by the equation shown in Table 2 or by using graphical method like the evaluation method based on temperature characteristic explained in Section 4.1. Therefore, the internal defects of cable joints can be effectively evaluated based on the thermal-mechanical characteristics under crimping process defect conditions.

5. Experimental Verification

5.1. Experiment Setup

In the above discussion, this article analyzes the influence of the contact coefficient k on the electromagnetic-thermal-mechanical characteristics of cable joints under crimping process defect conditions. In order to verify the accuracy of the proposed model, different experiments have been performed, and the experimental platform used was set up as follows: graphite rods are used to simulate the conductors of cable joints, and the resistance and current of the graphite rods are adjustable. In order to verify the accuracy of the thermal-mechanical characteristics of cable joints, the selected cable joint is simplified in the experiment to simulate the heat characteristics. Hence, an experimental setup as shown in Figures 19 and 21 is used to simulate the heat characteristics of cable joints under crimping process defects.

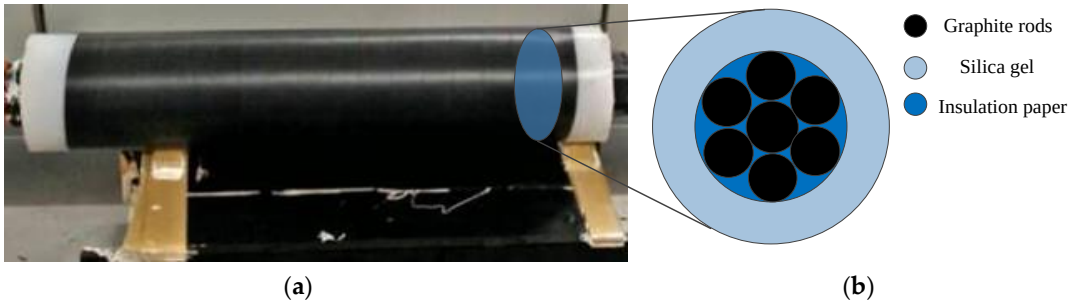

Figure 19. Simplified model of the cable joint, (**a**) The real model of the cable joint; (**b**) The structure of the cross section.

As shown in Figure 19, seven graphite rods with a radius of about 4.54 mm and length of 300 mm simulate the conductor of the cable joint and a silica gel layer with a thickness of 16.25 mm simulates the external insulating layer of the cable joint. Each graphite rod is isolated by insulation paper from the other graphite rods. The resistance of each graphite rod is 1 Ω. Figure 20 shows that a 12 V/30 A adjustable current source with a current range of 5 A to 30 A is applied to simulate the thermal loss caused by different contact resistances. An infrared imaging device (FLIR SC7000) is used to measure the surface temperature of the power cable in experiment. The graphite rods turn on and off can be controlled by the multiple channel switches, which simulate different thermal loss caused by internal defects in crimping process. The conduction modes of the different simplified cable joint model are shown in Figure 21.

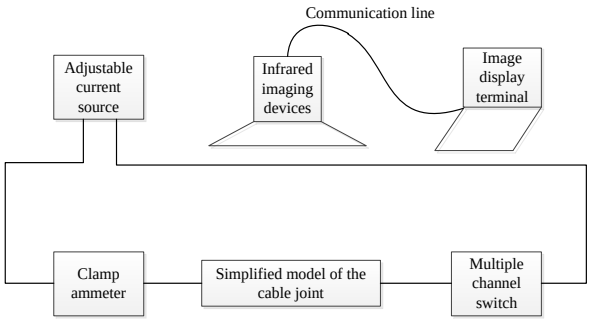

Figure 20. Experiment platform of the simplified cable joint model.

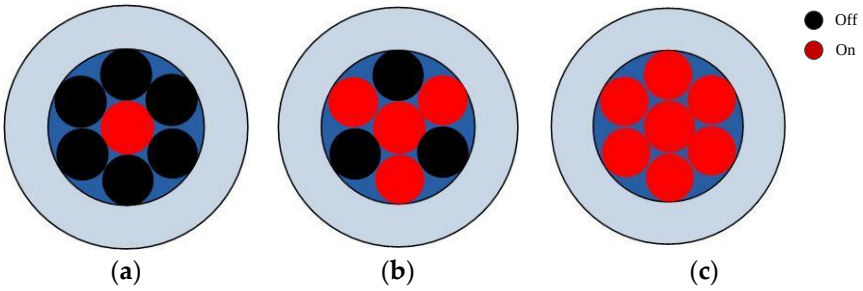

Figure 21. Conduction modes of the simplified cable joint model, (**a**) Single conductor on; (**b**) 4 conductor on; (**c**) 7 conductor on.

Due to the crimping process defects, the contact resistance of cable joints will rise, which causes the thermal losses density of cable joints to increase. Hence, we change the thermal loss density of the simplified cable joint model by changing the current flowing in the graphite rods to simulate the thermal losses caused by the crimping process defects.

According to the equation $P = I^2 \cdot R$, the heating power of the proposed cable joint model in different conduction modes with current range of 5 A to 30 A can be calculated in Table 3. Then according to the equation $I = \sqrt{P/R}$, we calculate the real load current of the cold-shrinkable joint of the 8.7/15 kV YJV 1 × 400 XLPE power cable at a certain equivalent resistance. Hence, this model simulates the different heating conditions of real cable with different contact coefficients k. This proposed work discusses the cable joint model working in a single conductor with a turn on and off technique with a current range of 5 A to 30 A.

Table 3. Heat power of the simplified cable joint model.

Conduction Modes	Minimum Heating Power/W	Maximum Heating Power/W
Single conductor on	25	900
Four conductors on	100	3600
Seven conductors on	170	6300

5.2. Results and Discussion

When the ambient temperature T_{amb} is 19 °C, a 15 A current is injected into the center graphite rod of the simplified cable joint model. After working for an hour, the surface temperature of the model can be measured as shown in Figure 22a. The surface temperature of the simplified cable joint model can be calculated by proposed method in this paper as shown in Figure 22b.

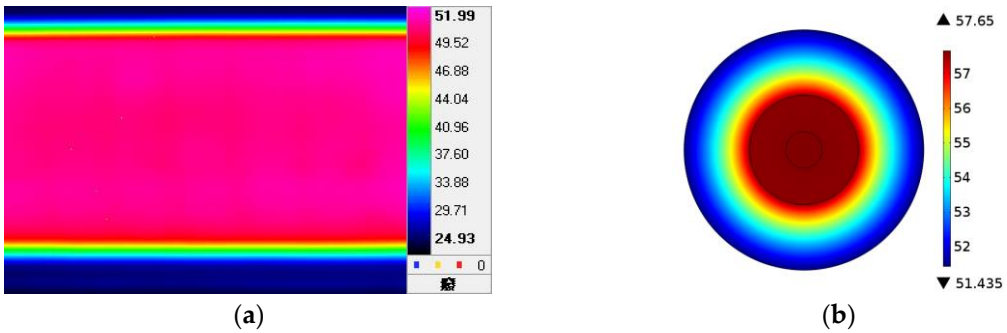

Figure 22. Comparison between the calculated temperature result and the experimental temperature result, (**a**) Experimental temperature result; (**b**) Calculation temperature result.

Figure 22 shows that the experimental temperature and calculation result of the simplified cable joint model are both about 51 °C and the computation results are identical with experimental results, which indicates that the electromagnetic-thermal-mechanical coupling model can be used to analyze the coupling field characteristics of cable joints under crimping process defect conditions and evaluate the crimping process internal defects of cable joints.

6. Conclusions

1. This paper establishes an electromagnetic-thermal-mechanical coupling analysis model based on the finite element method. The crimping process defects of cable joints are characterized by their contact resistances by solving the equivalent conductivity of the cable joint. Based on this model, the electromagnetic losses distribution, temperature distribution and stress distribution of a cable have been calculated.
2. Based on this model, the coupling fields characteristics for different contact coefficients k, ambient temperatures T_{amb} and load currents I were analyzed, which indicates that the internal defects of cable joints can be evaluated.
3. According to the thermal-stress characteristics of cable joints under internal defects, this paper uses the temperature difference ΔT_f and stress difference $\Delta \sigma_f$ of the cable surface to evaluate the internal defects of cable joints and proposes an evaluation method for internal defects of cable joints.
4. Simplified cable joint experiments which can simulate the temperature distribution of the cable and perform different defects tests are done and they verify the accuracy of the coupling field analysis model proposed in this paper.

Acknowledgments: This work was supported by the Fundamental Research Funds for Central Universities (No. CDJZR14155501), the National Natural Science Foundation of China (No. 51477013) and the science project of state grid headquarters (No. GYW17201600045). The authors would like to thank the anonymous reviewers for their instructive comments.

Author Contributions: This paper is a result of the collaboration of all co-authors. Fan Yang conceived and designed the study. Kai Liu was responsible for the modeling results and wrote most of the article. Peng Cheng and Bing Gao provided the theory for the modeling and established the model. Shaohua Wang and Xiaoyu Wang supervised the project and helped with most of the correction. Rong Xia designed all the experiments and revised the manuscript.

Conflicts of Interest: The authors declare no conflict of interest.

Nomenclature

μ	permeability
A	magnetic vector potential
σ	conductivity of cable joint
J_s	applied current density
ω	angular frequency
σ_{20}	conductivity at 20 °C
α	temperature coefficient
T	temperature
λ	thermal conductivity
Q_v	heat source per unit volume
h	coefficient of convective heat transfer
h_r	coefficient of radiation heat transfer
T_f	surface temperature
T_a	temperature of air
T_{amb}	ambient temperature
n	normal vector
σ_0	Stefan-Boltzmann constant
ε	surface emissivity
σ_1	conductivity of cable conductor
σ_2	equivalent conductivity

k	contact coefficient
I	load current
θ	stress tensor
f	externally applied force
ρ	material density
u	displacement
t	time
γ	damping coefficient
η	strain tensor
η^E	elastic strain component
η^{Th}	thermal strain component
D	strain coefficient
α	linear expansion coefficient
$E(T)$	young's modulus
v	Poisson's ratio of material
ΔT_f	surface temperature difference
$\Delta\sigma_f$	stress difference
T_{bf}	surface temperatures of cable body
T_{jf}	surface temperatures of cable joint

References

1. Cho, J.; Kim, J.-H.; Lee, H.-J.; Kim, J.-Y.; Song, I.-K.; Choi, J.-H. Development and Improvement of an Intelligent Cable Monitoring System for Underground Distribution Networks Using Distributed Temperature Sensing. *Energies* **2014**, *7*, 1076–1094. [CrossRef]
2. Benato, R.; Dambone Sessa, S.; Guglielmi, F.; Partal, E.; Tleis, N. Ground Return Current Behaviour in High Voltage Alternating Current Insulated Cables. *Energies* **2014**, *7*, 8116–8131. [CrossRef]
3. Benato, R.; Napolitano, D. Overall Cost Comparison Between Cable and Overhead Lines Including the Costs for Repair After Random Failures. *IEEE Trans. Power Deliv.* **2012**, *27*, 1213–1222. [CrossRef]
4. Benato, R.; Napolitano, D. State-space model for availability assessment of EHV OHL–UGC mixed power transmission link. *Electr. Power Syst. Res.* **2013**, *99*, 45–52. [CrossRef]
5. Stancu, C.; Notingher, P.; Ciuprina, F.; Notingher, P., Jr.; Castellon, J.; Agnel, S.; Toureille, A. Computation of the Electric Field in Cable Insulation in the Presence of Water Trees and Space Charge. *IEEE Trans. Ind. Appl.* **2009**, *45*, 30–43. [CrossRef]
6. Kroener, E.; Vallati, A.; Bittelli, M. Numerical simulation of coupled heat, liquid water and water vapor in soils for heat dissipation of underground electrical power cables. *Appl. Therm. Eng.* **2014**, *70*, 510–523. [CrossRef]
7. Olsen, R.; Anders, G.J.; Holboell, J.; Gudmundsdóttir, U.S. Modelling of Dynamic Transmission Cable Temperature Considering Soil-Specific Heat, Thermal Resistivity, and Precipitation. *IEEE Trans. Power Deliv.* **2013**, *28*, 1909–1917. [CrossRef]
8. Aras, F.; Alekperov, V.; Can, N.; Kirkici, H. Aging of 154 kV underground power cable insulation under combined thermal and electrical stresses. *IEEE Electr. Insul. Mag.* **2007**, *23*, 25–33. [CrossRef]
9. Mecheri, Y.; Boukezzi, L.; Boubakeur, A.; Lallouani, M. Dielectric and mechanical behavior of cross-linked polyethylene under thermal aging. In Proceedings of the Annual Report Conference on Electrical Insulation and Dielectric Phenomena, Victoria, CA, USA, 15–18 October 2000; pp. 560–563.
10. Tzimas, A.; Rowland, S.; Dissado, L.A.; Fu, M.; Nilsson, U.H. Effect of long-time electrical and thermal stresses upon the endurance capability of cable insulation material. *IEEE Trans. Dielectr. Electr. Insul.* **2009**, *16*, 1436–1443. [CrossRef]
11. Shaker, Y.O.; El-Hag, A.H.; Patel, U.; Jayaram, S.H. Thermal modeling of medium voltage cable terminations under square pulses. *IEEE Trans. Dielectr. Electr. Insul.* **2014**, *21*, 932–939. [CrossRef]
12. Gu, J.; Li, X.; Yin, Y. Calculation of electric field and temperature field distribution in MVDC polymeric power cable. In Proceedings of the IEEE International Conference Properties and Applications of Dielectric Materials, Harbin, China, 19–23 July 2009; pp. 105–108.
13. Choo, W.; Chen, G.; Swingler, S.G. Electric field in polymeric cable due to space charge accumulation under DC and temperature gradient. *IEEE Trans. Dielectr. Electr. Insul.* **2011**, *18*, 596–606. [CrossRef]

14. Illias, H.A.; Lee, Z.H.; Bakar, A.H.A.; Mokhlis, H.; Mohd Ariffin, A. Distribution of electric field in medium voltage cable joint geometry. In Proceedings of the International Conference on Condition Monitoring and Diagnosis (CMD), Bali, Indonesia, 23–27 September 2012; pp. 1051–1054.
15. Illias, H.A.; Ng, Q.L.; Bakar, A.H.A.; Mokhlis, H.; Ariffin, A.M. Electric field distribution in 132 kV XLPE cable termination model from finite element method. In Proceedings of the International Conference on Condition Monitoring and Diagnosis (CMD), Bali, Indonesia, 23–27 September 2012; pp. 80–83.
16. Lachini, S.; Gholami, A.; Mirzaie, M. The simulation of electric field distribution on cable under the presence of moisture and air voids. In Proceedings of the 4th International Power Engineering and Optimization Conference (PEOCO), Shah Alam, Malaysia, 23–24 June 2010; pp. 149–153.
17. Ying, Q.; Wei, D.; Gao, X.; Chen, P. Development of high voltage XLPE power cable system in China. In Proceedings of the 6th International Conference on Properties and Applications of Dielectric Materials, Xi'an, China, 21–26 June 2000; pp. 247–253.
18. Luo, J.; Shi, J.; Yuan, J. Study on Surface Discharge of Composite Dielectric in XLPE Power Cable Joints. *High Volt. Eng.* **2001**, *4*, 341–343.
19. Yoshida, S.; Tan, M.; Yagi, S.; Seo, S.; Isaka, M. Development of prefabricated type joint for 275 kV XLPE cable. In Proceedings of the IEEE International Symposium on Electrical Insulation Conference, Toronto, ON, Canada, 3–6 June 1990; pp. 290–295.
20. Anders, G.J.; Chaaban, M.; Bedard, N.; Ganton, R.W.D. New Approach to Ampacity Evaluation of Cables in Ducts Using Finite Element Technique. *IEEE Trans. Power Deliv.* **1987**, *285*, 969–975. [CrossRef]
21. Chatziathanasiou, V.; Chatzipanagiotou, P.; Papagiannopoulos, I.; De Mey, G.; Więcek, B. Dynamic thermal analysis of underground medium power cables using thermal impedance, time constant distribution and structure function. *Appl. Therm. Eng.* **2013**, *60*, 256–260. [CrossRef]
22. Sedaghat, A.; De Leon, F. Thermal Analysis of Power Cables in Free Air: Evaluation and Improvement of the IEC Standard Ampacity Calculations. *IEEE Trans. Power Deliv.* **2014**, *29*, 2306–2314. [CrossRef]
23. Canova, A.; Freschi, F.; Giaccone, L.; Guerrisi, A. The high magnetic coupling passive loop: A steady-state and transient analysis of the thermal behavior. *Appl. Therm. Eng.* **2012**, *37*, 154–164. [CrossRef]
24. Anders, G.J.; Coates, M.; Chaaban, M. Ampacity Calculations for Cables in Shallow Troughs. *IEEE Trans. Power Deliv.* **2010**, *25*, 2064–2072. [CrossRef]
25. Pilgrim, J.A.; Lewin, P.L.; Larsen, S.T.; Waite, F.; Payne, D. Rating of Cables in Unfilled Surface Troughs. *IEEE Trans. Power Deliv.* **2012**, *27*, 993–1001. [CrossRef]
26. Yang, F.; Cheng, P.; Luo, H.; Yang, Y.; Liu, H.; Kang, K. 3-D thermal analysis and contact resistance evaluation of power cable joint. *Appl. Therm. Eng.* **2016**, *93*, 1183–1192. [CrossRef]